Title: Anodic respiration of *Pseudomonas putida* KT2440 in a stirred-tank bioreactor

Author: Sarah Hintermayer Shiqin Yu Jens O. Krömer Dirk Weuster-Botz

PII: S1369-703X(16)30211-X
DOI: http://dx.doi.org/doi:10.1016/j.bej.2016.07.020
Reference: BEJ 6531

To appear in: *Biochemical Engineering Journal*

Received date: 18-4-2016
Revised date: 8-7-2016
Accepted date: 30-7-2016

Please cite this article as: Sarah Hintermayer, Shiqin Yu, Jens O.Krömer, Dirk Weuster-Botz, Anodic respiration of Pseudomonas putida KT2440 in a stirred-tank bioreactor, Biochemical Engineering Journal http://dx.doi.org/10.1016/j.bej.2016.07.020

Title:

Anodic respiration of *Pseudomonas putida* KT2440 in a stirred-tank bioreactor

Authors:

Sarah Hintermayer, Shiqin Yu, Jens O. Krömer and Dirk Weuster-Botz

Author affiliation:

Sarah Hintermayer and Dirk Weuster-Botz:

Institute of Biochemical Engineering, Technical University of Munich,

Boltzmannstr. 15, 85748 Garching, Germany

Shiqin Yu and Jens O. Krömer:

Centre for Microbial Electrochemical Systems (CEMES) and Advanced Water Management Centre (AWMC), Level 4, Gehrmann Bldg (60)

The University of Queensland, Brisbane, QLD 4072, Australia

Corresponding author:

Dirk Weuster-Botz

Phone: +49 (0)89 289 15712; Fax: +49.89.289.15714

E-Mail: d.weuster-botz@lrz.tum.de

Graphical Abstract

Controlling the redox potential in the medium is important to achieve steady *para*-hydroxybenzoate (*p*HBA) production in a bio-electrochemical system with *Pseudomonas putida* KT2440 ΔpobA/pSEVA-*ubiC*. The working electrode potential did not influence the anodic respiration but the ratio of oxidized to reduced mediator concentration did. Using a fully controlled stirred-tank bioreactor with redox potential control of the medium, *p*HBA concentration could be increased by 69 % compared to the aerobic process and current densities of 12.5 mA cm^{-2} were reached.

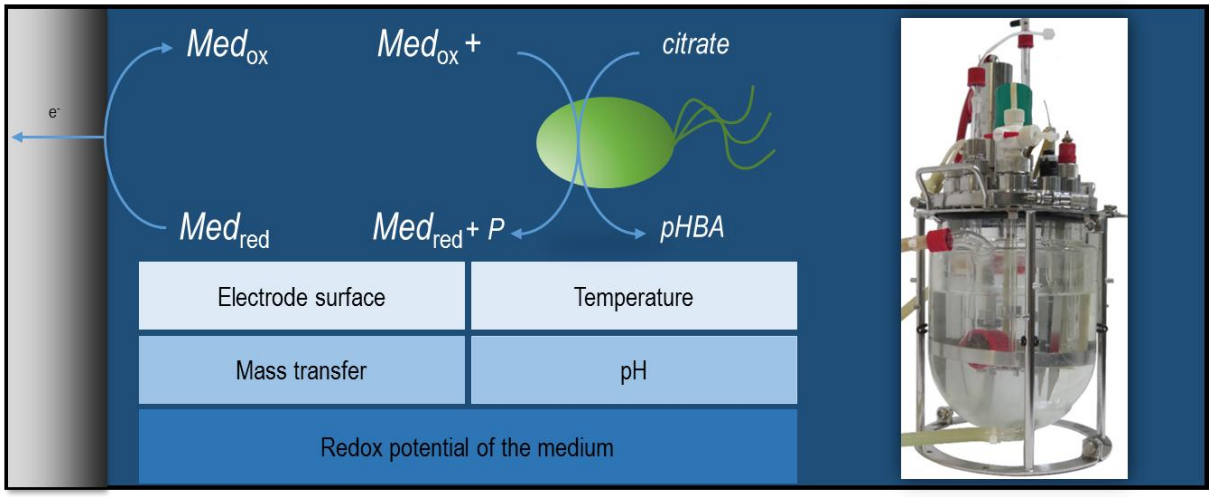

Highlights

- A fully controlled stirred-tank bioreactor was used as a bio-electrochemical system.
- Electro-fermentative *para*-hydroxybenzoic acid production was optimised.
- Mass transfer limits production rates in the electro-fermentative process.

- Redox potential in the medium needs to be controlled.

- *para*-Hydroxybenzoic acid yields exceeded *p*HBA yields from an aerobic batch process.

Abstract

Anodic batch production of *para*-hydroxybenzoic acid (*p*HBA) from citric acid with a genetically modified *Pseudomonas putida* KT2440 strain was studied in a bio-electrochemical system (BES) based on a standard lab-scale stirred-tank bioreactor at fully controlled anaerobic reaction conditions. Electron transfer to the anode was mediated by addition of $K_3Fe(CN)_6$ to the medium. Effects of varying anode surface areas (graphite rod, felt and brush), power input (stirrer speed) and mediator concentrations were investigated. The obligate aerobic *P. putida* grew anaerobically with mediated anodic respiration and *p*HBA production was observed. Anodic respiration was best applying the graphite rod electrode which showed a maximal current density of 12.5 mA cm^{-2}. This is the highest measured for non-porous electrodes in BES until now. Increasing the power input to 2.93 W L^{-1} (700 rpm) and online control of the redox potential E_{Medium} at 225 mV (vs. Ag/AgCl) in the medium by controlled addition of mediator resulted in a maximal *p*HBA yield of 9.91 $mmolC_{pHBA}$ $molC^{-1}_{citrate}$ which exceeds *p*HBA yields in the aerobic batch process by 69 % (5.87 $mmolC_{pHBA}$ $molC^{-1}_{citrate}$).

Keywords: *Pseudomonas putida* KT2440, bio-electrochemical system (BES), anodic production, *para*-hydroxybenzoic acid, redox potential, mass transfer.

1 Introduction

Innovative fermentation processes are necessary for cost-effective bio-production of chemicals [1]. Fermentation processes are operated under aerobic or anaerobic conditions. Aerobic processes have a high energy demand for intensive aeration of the fermentation broth. Anaerobic processes can be operated with lower energy input but show formation of unwanted by-products [2]. Microorganisms form by-products to balance their redox metabolism [3] which reduces yields and can cause product inhibition [4–6]. An alternative may be offered by electro-fermentation, where an electrode provides an electron source or sink to overcome bottlenecks or drive fermentations towards particular desired products [7,8]. In such bio-electrochemical processes the redox metabolism can be balanced by external electron transfer between the microorganism and an electrode as electron acceptor (anodic process) or donor (cathodic process) under anaerobic conditions. Electro-fermentation has shown to be effective at increasing the synthesis of several products including ethanol, n-butanol and succinate with a variety of microorganisms such as *Saccharomyces cerevisiae*, *Clostridium acetobutylicum* or *Actinobacillus succinogenes* [9–12]. In contrast to all other electron acceptors or donors that can be utilised by microorganisms, electrodes cannot be depleted. Thus they offer the possibility of developing anaerobic production pathways that do not need to be stoichiometrically balanced with respect to the oxidation states of substrates and products [13].

Para-hydroxybenzoic acid (*p*HBA) is a high value intermediate in the shikimate pathway which is used for the production of poly-crystal polymers [14]. So far *p*HBA has been produced under aerobic conditions from glucose in recombinant strains of *Escherichia coli* [15], *Saccharomyces cerevisiae* [16,17] and *Pseudomonas putida* [18,19]. Maximal *p*HBA yields of 49 $mmolC_{pHBA}\ molC^{-1}_{glucose}$ were achieved with *P. putida* in a chemostat cultivation

[19]. *P. putida* may be a preferred production host for *p*HBA because of its high tolerance to aromatic compounds [20,21].

Bio-electrochemical systems in which microbial redox reactions are performed consist of an anodic and a cathodic chamber that are separated by a membrane [22]. When the oxidation of organic matter by microorganisms takes place in the anodic chamber, the process is referred to as anodic respiration. Anodic respiration requires electron transfer from the microorganism towards an external acceptor. External electron transfer, the central feature of electrogenic microorganisms, can occur by two different mechanisms [23]. Firstly, microorganisms can be directly attached to electrode surfaces forming electro-active biofilms. The direct electron transfer can occur via redox proteins in the membrane or pili-like structures, the so called nanowires. Secondly, redox mediators dissolved in the aqueous phase can shuttle electrons from the microorganism towards the electrode. Natural redox mediators can be produced by the microorganism or artificial mediators can be added. The major advantage of mediators is the enlargement of the reaction space so that electrochemical reactions can take place not only at the electrode surface but also in the bulk medium. It was previously observed that ferricyanide can serve as electron acceptor during the oxidation of nicotinic acid by *Pseudomonas fluorescens* [24] and the oxidation of glucose by *Pseudomonas putida* F1 [25].

Bio-electrochemical reactor systems described so far in literature vary strongly with respect to geometries, were not well mixed and important state variables (e.g. pH) were not controlled [26]. Modification of stirred-tank bioreactors in order to establish bio-electrochemical systems could be beneficial for mediated bio-electrochemical processes because stirred-tank bioreactors can easily be scaled-up and are very well established in industry.

This paper deals with the application of a commercially available standard stirred-tank bioreactor for mediated anodic respiration with all modifications being reversible. Anodic

batch production of *p*HBA from citric acid with *Pseudomonas putida* KT2440 with overexpression of the chorismate-pyruvate lyase gene and knock-out of the 4-hydroxybenzoate 3-monooxygenase gene will be studied at fully controlled reaction conditions. Investigations will be focused on potentially limiting process variables such as electrode surface area, power input (stirrer speed) and mediator concentrations (potassium ferricyanide). The bio-electrochemical process performance of the recombinant *Pseudomonas putida* KT2440 will be compared to the aerobic batch process in a standard stirred-tank bioreactor.

2 Materials and methods

2.1 Microorganism and strain construction

Pseudomonas putida KT2440 was engineered to produce *p*HBA by knocking out *pobA* encoding for 4-hydroxybenzoate 3-monooxygenase (EC 1.14.13.2). This disrupts the conversion of *p*HBA to 3,4-dihydroxybenzoic acid and thus prevents *p*HBA degradation via the ortho-cleavage pathway. Furthermore, the strain was transformed with the vector pSEVA2345 for overexpression of the gene *ubiC,* which encodes the enzyme chorismate-pyruvate lyase converting chorismate to *p*HBA and pyruvate.

2.2 Strain construction

The *ubiC* gene was artificially synthesized based on the amino acid sequence from *Escherichia coli* K-12 substr.W3110 (CAA40681.1) and expression was induced by IPTG. Genetic engineering was applied using the pEMG/pSW-2 system [27].The 500bp-800bp upstream and downstream sequences of the gene *pob*A were amplified with the primer pairs KTKO PobA P1/ KTKO PobA P3 and KTKO PobA P4/ KTKO PobA P6. In the following the primer pair KTKO PobA P2/ KTKO PobA P5 was used to fuse the gene upstream and downstream of the *pobA* sequence.

The resulting fusion gene was digested with EcoR I/ BamH I, and inserted into the vector pEMG resulting in the plasmid pMEG-Δ*pobA*, which was further transformed into *P. putida* KT2440. The plasmid integrated into the chromosome which was confirmed by colony PCR. Then the second plasmid containing an I-SceI endonuclease was introduced into the resulting strain and induced with 15 mM 3-methylbenzoate to remove the pEMG backbone. The resulting strains were identified using colony PCR.

The construction of overexpression plasmid was done by a restriction enzyme digest and ligation approach. The gene *ubiC* was inserted into EcoR I/ Hind III of the vector pSEVA234 [28], resulting in the plasmid pSEVA234-*ubiC*.

All constructions were confirmed by sequencing (Australian Genome Research Facility, St Lucia, Australia). The expression plasmid pSEVA234-*ubiC* was electro-transformed into the mutant *P. putida* Δ*pob*A following Choi's protocol [29], generating the strain of *P. putida* Δ*pob*A/ pSEVA234-*ubiC*.

2.3 Medium, chemicals and reagents

LB medium with 10 g L^{-1} peptone (Appli Chem, Darmstadt, Germany), 5 g L^{-1} yeast extract (Deutsche Hefewerke, Nuremberg, Germany), 10 g L^{-1} NaCl (Carl Roth, Karlsruhe, Germany) and 50 µg mL^{-1} kanamycin (Carl Roth, Germany) was used for the cultivation of *Pseudomonas putida* KT2440 Δ*pobA*/pSEVA-*ubiC* in test tubes. A defined medium was applied in shake flasks and in fully controlled stirred-tank bioreactors with 5 g L^{-1} citrate (Carl Roth, Germany), 6 g L^{-1} Na_2HPO_4 (neoLab, Heidelberg, Germany), 3 g L^{-1} KH_2PO_4 (Carl Roth, Germany), 1 g L^{-1} NH_4Cl (neoLab, Germany), 0.1 g L^{-1} $MgSO_4 \cdot 7\ H_2O$ (Carl Roth, Germany), 0.015 g L^{-1} $CaCl_2 \cdot 2\ H_2O$ (Merck, Darmstadt, Germany), 1 mM isopropyl-β-D-thiogalactopyranoside (IPTG, Carl Roth, Germany), 50 µg mL^{-1} kanamycin (Carl Roth, Germany) and 1 mL L^{-1} of a trace elements stock solution containing 1.5 g L^{-1} $FeCl_3 \cdot 6\ H_2O$ (Merck, Germany), 0.15 g L^{-1} H_3BO_3 (Merck, Germany), 0.03 g L^{-1} $CuSO_4 \cdot 5\ H_2O$ (Merck,

Germany), 0.18 g L^{-1} KI (Merck, Germany), 0.12 g L^{-1} $MnCl_2 \cdot 4\ H_2O$ (VWR, Radnor, PA, USA), 0.06 g L^{-1} $Na_2MoO_4 \cdot 2\ H_2O$ (Merck, Germany), 0.12 g L^{-1} $ZnSO_4 \cdot 7\ H_2O$ (Merck, Germany), 0.15 g L^{-1} $CoCl_2 \cdot 6\ H_2O$ (Merck, Germany), 10 g L^{-1} EDTA (acid form) (Carl Roth, Germany), 0.023 g L^{-1} $NiCl_2 \cdot 6\ H_2O$ (Merck, Germany). The mediator potassium ferricyanide (Alfa Aesar, Karlsruhe, Germany) was applied at an initial concentration of 3 mM in electro-fermentations if not stated otherwise. Media were sterilised at 121 °C for 20 min. $CaCl_2 \cdot 2\ H_2O$, $K_3Fe(CN)_6$, IPTG and kanamycin were filter sterilized and added after sterilisation. Traces of oxygen were stripped with nitrogen gas for at least 12 h before inoculation of electro-fermentations. The electrolyte for cathode chamber and glass bridge tube was the defined medium without citrate.

All restriction enzymes, ligase and polymerase were purchased from New England Biolabs (Ipswich, MA, USA). Plasmid extraction and PCR product purification was done using GeneJET Plasmid Miniprep Kit and GeneJET PCR Purification Kit, respectively (Thermo Fisher Scientific, Australia). All DNA manipulation was followed according to the suppliers' recommendation.

2.4 Stirred-tank based bio-electrochemical reactor

A 1.8 L autoclavable stirred-tank bioreactor made of glass (Labfors, Infors, Bottmingen, Switzerland) was modified to operate the reactor as an electrically insulated bio-electrochemical cell. The stainless steel lid with all openings for probes, agitator shaft, sampling and fluid connectors was electrically isolated from the metal rack by a silicone ring. All electrically conductive connections between the lid and the reaction medium were replaced by non-conductive materials. The stainless steel agitator shaft was replaced by an agitator shaft made from polyether-etherketone (PEEK) (diameter 12 mm). This shaft was equipped with two Rushton turbines (Figure 1). The original stainless steel immersion tube for the temperature probe was replaced by an immersion tube made out of PEEK. The

original stirred tank baffles (stainless steel) did not reach the lid and were therefore used without modification. Visually, no corrosion effects were observed over a period of 1.5 years of operation. Gassing and sampling was realised by glass tubes with an inner diameter of 6 mm (outer diameter 9 mm). A three-way valve at the top of the sampling tube reduced the discarded sampling volume to a minimum, which is important at long process durations. The working electrode was fixed on a PEEK rod which had an opening of 1 mm for the titanium wire (Grade 2, diameter 0.6 mm, Ankuro Int., Rostock, Germany) to which the working electrode was connected. Graphite rod (MBM, Hofheim, Germany), graphite felt (CGC Klein, Siegen, Germany) and graphite brush (The Mill-Rose Company, Mentor, OH, USA) electrodes were used as working electrodes. The working electrode was placed next to the glass bridge tube (Figure 1 F, G) of the reference electrode (Ag/AgCl reference electrode, IJ Cambria Scientific, Llanelli, United Kingdom). Opposite, resulting in a triangular electrode arrangement, the cathode chamber was positioned. The cathode chamber (Figure 1 D, E) was made out of glass. Catholyte and anolyte were separated by a cation exchange membrane (CMI-7000, Membranes International, Ringwood, NJ, USA, oxygen diffusion coefficient = 3.72 10^{-5} m^2 d^{-1} [30]) which was fixed by a GL 32 screw cap with a 2 cm diameter opening. The membrane area was 3.14 cm^2. Cation exchange membranes are permeable for protons generated in the anodic chamber [31]. To avoid acidification of the catholyte by these protons, the catholyte was gassed with air in order to supply oxygen for the cathode chamber reaction (2 O_2 + 8 H^+ + 8 e^- → 4 H_2O) [32]. The oxygen diffusion flux from the cathode to the anode chamber at 30 °C was estimated to be 0.012 mmol O_2 d^{-1} and could therefore be neglected. As cathode material titanium gauze (18 mesh woven from 0.28 mm diameter wire, Alfa Aesar, Karlsruhe, Germany) was used. All components, glass or metal, were fixed by commercially available adapters from Infors (Bottmingen, Switzerland).

To minimize disturbances of potentiostatic measurements the agitator drive was earthed and insulated against the reactor lid using insulating tape (Coroplast, Fritz Müller, Wuppertal, Germany) which was mounted after sterilisation. To minimize evaporation from both the anodic as well as the cathodic chamber the inlet gas was saturated with water. Nevertheless the electrolyte of the cathode chamber had to be replenished periodically.

Online measurement of the redox potential in the anodic chamber was done using a redox electrode (Redox-Gold OPS32-0NBO2GSA, Eurotronic Umwelttechnik, Gersfeld, Germany). Anodic electro-fermentations with redox electrode were performed with a 3.6 L glass vessel (Labfors, Infors, Bottmingen, Switzerland) modified in the same way as described before, because an additional opening was necessary for the redox probe.

2.5 Fermentations

Electro-fermentations were carried out in batch mode making use of the fully controlled 1.8 L stirred-tank based bio-electrochemical reactor with a working volume of 1 L. The stirrer was initially operated at 400 rpm (volumetric power input 0.61 W L^{-1}). The pH was measured online with a pH probe (400-DASP-SC-K8S/200, Mettler Toledo, Columbus, OH, USA) and controlled with NH_4OH (28 % (v/v)) and H_3PO_4 (12.5 % (v/v)) (AppliChem, Darmstadt, Germany). Temperature and pH were controlled at 30 °C and 7.0, respectively. The reactor was continuously stripped with nitrogen at a constant flow rate of 0.1 L min^{-1} to ensure strictly anaerobic conditions during the fermentation. Antifoam (Struktol, Schill-Seilacher, Hamburg, Germany) was added manually as required. Stirrer speed, pH, temperature and nitrogen flow were controlled with a Labfors operation unit (Infors, Bottmingen, Switzerland) which provided a galvanically insulated circuit for pH measurement. The working electrode potential was controlled at +0.500 V (vs. Ag/AgCl) by a potentiostat (SP-150/Z, Bio-Logic, Claix, France). The redox potential in the medium was controlled by automated feeding of a 1 M $K_3Fe(CN)_6$ stock solution. The feed pump of the Labfors

operation unit (Infors, Bottmingen, Switzerland) was actuated with a feedback control that was realised by a sequence directly implemented in the IRIS software (version 5.2; Infors, Bottmingen, Switzerland). The processes with redox potential control were conducted in the 3.6 L reactor with a working volume of 2.5 L. The working electrode was identical with the electrode used in the 1.8 L reactor. The ratio of geometric surface area of the working electrode to reactor volume were 18.98 cm^2 L^{-1} (1.8 L reactor) and 7.59 cm^2 L^{-1} (3.6 L reactor).

Aerobic fermentations were carried out in the fully controlled 1.8 L stirred-tank bioreactor under identical conditions with the exception that the reactor was gassed with 1 L min^{-1} of sterile air. The dissolved oxygen concentration was kept above 30 % by automatic increases of stirrer speed.

The inoculum for aerobic and electro-fermentations was prepared in aerobic shake flasks. Expression of *ubiC* in the shake flasks was induced during the exponential phase followed by 7 h of induced growth. It was first centrifuged (4500 rpm, 20 min) and the pellet washed with sterile PBS (8.0 g L^{-1} NaCl (Carl Roth, Karlsruhe, Germany), 0.2 g L^{-1} KCl (Merck, Darmstadt, Germany), 1.44 g L^{-1} Na_2HPO_4 (neoLab, Heidelberg, Germany), 0.24 g L^{-1} KH_2PO_4 (Carl Roth, Germany)). The initial optical density in the stirred-tank reactor was fixed to OD_{600} = 0.3.

2.6 Analytical methods

Cell growth was monitored offline by measuring the optical density at 600 nm (Genesys 20, Thermo Electron, Karlsruhe, Germany). Cell dry weight concentrations were calculated from OD_{600} according to $c_{\mathrm{CDW}} = 0.577 \cdot OD_{600}$. Sterile filtered liquid samples were withdrawn to measure substrate, product and by-product concentrations by high-performance liquid chromatography (Agilent 1100 Series, Agilent, Santa Clara, CA, USA) equipped with an refractive index (RI) detector (Agilent 1200 Series, Agilent), UV/VIS detector (S3300,

Sykam, Eresing, Germany) and an Aminex HPX-87H column (Bio-Rad, Munich, Germany) for the detection of organic acids. The column was operated at 60 °C with a constant flow rate of 0.7 mL min^{-1} (eluent: 5 mM sulfuric acid). The retention time for citrate was 6.9 min, for malate 8.1 min, for fumarate 11.5 min and for *p*HBA 42 min. Sterile filtered samples were used to measure the extinction of the oxidised mediator ($K_3Fe(CN)_6$) at 420 nm. To determine its concentration the molar attenuation coefficient ε = 1040 M^{-1} cm^{-1} [33] was used. The overall concentration of $K_3Fe(CN)_6$ was determined after total oxidation of 160 µL sterile filtered sample with 20 µL HCl (37 % (w/w)) and 10 µL H_2O_2 (30 % (w/w)) in 610 µL PBS at 420 nm. From both measurements the amount of reduced mediator ($K_4Fe(CN)_6$) could be determined. Brunauer-Emmett-Teller (BET) measurements were performed after drying the electrode materials at 100 °C for 24 h under vacuum. Measurements were done with N_2 and a BET surface area analyser (Gemini VII, Micromeritics, Aachen, Germany).

2.7 Reaction engineering analysis

Substrate, dry cell mass and metabolite concentrations as well as reactor volume data were measured off-line. The sigmoidal Richards function [34] was applied to interpolate biomass, *p*HBA and substrate concentrations as a function of process time in the batch processes. Specific growth rates ($\mu = c_X^{-1}\, dc_X\, dt^{-1}$), substrate uptake rates ($q_S = -\, c_X\, dc_S\, dt^{-1}$) and biomass yields ($Y_{XS} = \mu\, q_S^{-1}$) were calculated with the interpolated biomass and substrate concentrations. From exhaust gas data measured online, cell specific oxygen consumption (q_{O2}) and carbon dioxide production (q_{CO2}) rates were calculated.

2.7.1 Interpolation of biomass, product and substrate concentrations

Biomass and product concentrations (c_i; i = X (biomass) or i = P (product)) were interpolated with the Richards function:

$$c_i(t) = a \cdot \left(1 + (d-1) \cdot e^{-k\cdot(t-b)}\right)^{\frac{1}{1-d}} \qquad 1$$

Parameter *a* is the upper horizontal asymptote, *b* is the abscissa of the inflection point, *d* defines the asymmetry of the sigmoidal curve about its inflection point, *k* is the horizontal stretch factor, and *t* is the process time.

Substrate concentrations (c_S) were interpolated with equation 2 which was derived from equation 1 by mirroring it in the abscissa and vertically shifting it by *a*.

$$c_S(t) = a \cdot \left(1 - \left(1 + (d-1) \cdot e^{-k \cdot (t-b)}\right)^{\frac{1}{1-d}}\right) \quad (2)$$

The Levenberg-Marquardt algorithm (Matlab statistics toolbox, MATLAB R2013a, Mathworks, USA) was used for parameter estimation of equation 1 and 2 by minimizing the residual sum of squares of biomass and substrate concentrations as function of process time.

2.7.2 Exhaust gas analytics

From exhaust gas data measured online, cell specific oxygen consumption (q_{O2}, equation 3) and carbon dioxide production (q_{CO2}, equation 4) rates were calculated (V_{gas}^{in}: inlet air flow; x_i^{in}: mole fraction of component *i* at the inlet; x_i^{out}: mole fraction of component *i* at the outlet; V_{mol}: molar volume of an ideal gas 22.414 L mol^{-1}; V_R: volume, $\overline{c}_{CDW}$: mean cell dry weight concentration).

$$q_{O_2} = \frac{V_{gas}^{in}}{V_R \cdot V_{mol} \cdot \overline{c}_{CDW}} \left(x_{O_2}^{in} - \frac{1 - x_{CO_2}^{in} - x_{O_2}^{in}}{1 - x_{CO_2}^{out} - x_{O_2}^{out}} \cdot x_{O_2}^{out} \right) \quad (3)$$

$$q_{CO_2} = \frac{V_{gas}^{in}}{V_R \cdot V_{mol} \cdot \overline{c}_{CDW}} \left(\frac{1 - x_{CO_2}^{in} - x_{O_2}^{in}}{1 - x_{CO_2}^{out} - x_{O_2}^{out}} \cdot x_{CO_2}^{out} - x_{CO_2}^{in} \right) \quad (4)$$

2.7.3 Carbon and electron balances

Carbon and electron balances were determined by equations 5 to 8.

$$Carbon\ balance = \frac{n_t(C_{total})}{n_0(C_{total})} \quad (5)$$

$$n_t(C_{total}) = n_t(C_{Reactor}) + \sum_0^t n_t(C_{CO_2}) + \sum_0^t n_t(C_{Sample}) \quad (6)$$

$n_t(C_{total})$: total mole carbon that could be recovered at time *t;* $n_t(C_{Reactor})$: mole carbon present in the reactor at time *t;* $\sum_0^t n_t(C_{CO_2})$: cumulated mole carbon in form of CO_2 measured by exhaust gas analytics; $\sum_0^t n_t(C_{Sample})$: cumulated mole carbon found in samples until time *t*.

$$Electron\ balance = \frac{n_{t,e^-}}{n_{0,\,e^-}} \quad (7)$$

$$n_{t,e^-} = \kappa_X \cdot n_t(C_X) + \sum_{i=1}^{M} \kappa_{P,i} \cdot n_t(C_{P,i}) + \sum_{i=1}^{N} \kappa_{S,i} \cdot n_t(C_{S,i}) + \frac{Q_t}{F} + n_t(C_{K4Fe(CN)6}) \cdot z \quad (8)$$

κ_X: degree of reduction of biomass (4.31 mol_{e^-} $molC^{-1}_X$; calculated based on the biomass composition published by 35 [35], 36 [36], and the element valences published by 37[37]); $\kappa_{P,i}$: Degree of reduction of product *i*; $\kappa_{S,i}$: degree of reduction of converted substrate *i*; $\Delta n_t(C_i) = \Delta n_{t=0}(C_i) - \Delta n_t(C_i)$ in mol C_i. The last two addends in equation 8 were only used in electro fermentations, they describe the electrons transferred to the electrode *(Q:* charge, C; *F*: Faraday constant, 96485.3 C mol^{-1}) and the electrons stored in the reduced mediator species (z: number of moles of electrons per mole $K_4Fe(CN)_6$; z = 1).

The reactor mass was measured gravimetrically throughout the batch process to consider volume reductions due to evaporation and sampling. The mass of the medium was obtained by subtracting the tare weight of the reactor from the measured reactor mass. The density of water at 30 °C (995 kg m^{-3}) was used to calculate the reactor volume. The reactor volume at time *t* ($V_{Reactor,t}$) is given by the initial reactor volume at time *t* = 0 ($V_{Reactor,t_0}$) minus the volume reduction caused by evaporation ($V_{Evaporation,t}$) and sampling ($\sum_0^t V_{Sample,t}$):

$$V_{Reactor,t} = V_{Reactor,t_0} - V_{Evaporation,t} - \sum_0^t V_{Sample,t} \quad (9)$$

3 Results and Discussion

In this study citrate was used to evaluate the anodic *p*HBA formation with *P. putida* KT2440. Preliminary tests on *p*HBA formation with *P. putida* in a bio-electrochemical system had shown that no *p*HBA was formed when glucose and glycerol were used as substrates (data not shown). With citrate as substrate *p*HBA formation was possible. In anodic electro-fermentations with *P. putida* F1 it had been shown that during the anodic oxidation of glucose with *P. putida* F1 a NADPH shortage occurred [25]. Because *P. putida* F1 and *P. putida* KT2440 are very similar a NADPH shortage could have prevented *p*HBA formation with glucose and possibly from glycerol. Intracellular NADPH concentrations were not determined in this study.

3.1 Aerobic *p*HBA production

In aerobic cultivation of *P. putida* KT2440 Δ*pobA*/pSEVA-*ubiC*, citrate depletion occurred within 6 h after inoculation (Figure 2 A). A final biomass concentration of 2.3 g L^{-1} (0.44 $molC_X\ molC^{-1}_{citrate}$) was measured (Figure 2 B). The maximal *p*HBA concentration was 20.6 mg L^{-1}, which equals a yield of 5.87 $mmolC_{pHBA}\ molC^{-1}_{citrate}$ (Figure 2 C). By the end of the cultivation 0.09 mol CO_2 had been formed (0.56 $molC_{CO2}\ molC^{-1}_{citrate}$) resulting in closed carbon (98.9 %) and electron (99.6 %) balances (Figure 2 M, N).

Citrate was metabolised with a maximal substrate uptake rate of 8.29 mmol $(g_X\ h)^{-1}$ (Figure 2 D. The growth rate remained constant at 0.63 h^{-1} (Figure 2 E). The maximal *p*HBA formation rate was 0.05 mmol $(g_X\ h)^{-1}$ (Figure 2 F). The specific oxygen uptake rate reached a maximum of 25.4 mmol $(g_X\ h)^{-1}$ after 1.8 h and decreased thereafter (Figure 2 J). The induction with IPTG (Figure 2 I) resulted in a decrease of the specific carbon dioxide formation rate from 31.5 mmol $(g_X\ h)^{-1}$ to 20.2 mmol $(g_X\ h)^{-1}$ (Figure 2 K). The respiratory quotient (*RQ*) was observed to be between 1 mol mol^{-1} and 3 mol mol^{-1} (Figure 1 L). CO_2 and

biomass were the major products of the aerobic conversion of citrate with *P. putida* Δ*pobA*/pSEVA-*ubiC* as can be seen by the high CO_2 and biomass yields.

3.2 Working electrodes for mediated anodic respiration

The working electrode is a central component of any bio-electrochemical system. During anodic respiration the working electrode serves as the terminal electron sink. It has already been shown that *P. putida* F1 requires the presence of a mediator that possesses a mid point potential above 0 V (vs. Ag/AgCl). In a preliminary study potassium ferricyanide (mid point potential of 0.21 V (vs. Ag/AgCl)) and riboflavin (mid point potential of -0.44 V (vs. Ag/AgCl)) were evaluated as mediators for *P. putida* KT2440. In consistence with published results with *P. putida* F1 [25], the current observed with *P. putida* KT2440 and riboflavin was negligibly small compared to the current observed with $K_3Fe(CN)_6$ (data not shown). Therefore $K_3Fe(CN)_6$ was used as a mediator in all experiments.

The mediator shuttles electrons from the bulk or from a biofilm developed on the electrode surface. In either case it is important that the mediator is efficiently oxidised to ensure unlimited external electron transfer for the microorganisms. The formation of a biofilm changes the electrode surface area accessible to the mediator and its diffusion to the electrode surface.

In order to identify an electrode that ensures unlimited external electron transfer and reduces biofilm formation graphite rod, brush and felt electrodes were examined in electro-fermentations of *P. putida* KT2440 Δ*pobA*/pSEVA-*ubiC*. The electrodes under study had the same electrical properties as they were all made out of the same material but differed markedly in their geometries and surface areas (Table 1). Surface areas were determined by Brunauer-Emmett-Teller (BET) measurements. The specific surface areas of the brush and felt electrode were 299 $m^2\ kg^{-1}$ and 409 $m^2\ kg^{-1}$, respectively. The surface area of the rod

electrode was too small to be measured by the BET method, therefore it was estimated geometrically and gravimetrically (0.750 m^2 kg^{-1}).

During the electro-fermentations visually observable biofilm was formed only on the brush and felt electrodes (Table 1). The largest increase of suspended biomass (0.06 g L^{-1}) was observed for the rod electrode (Figure 3 D). The maximal currents were 2.48 mA (rod electrode), 2.47 mA (brush electrode) and 6.35 mA (felt electrode). This clearly showed that increasing the specific electrode surface area by 40 000 % (brush electrode) and 55 000 % (felt electrode) in comparison to the rod electrode reduced the current in the case of the brush electrode and only increased the current by a factor of 2.5. Current densities (*j*) were determined with regard to the projected surface area since this is the most frequently used reference [38]. The highest current density was obtained with the rod electrode (0.47 mA cm^{-2}) although this electrode has the smallest surface by any measure (Figure 3 J). Maximal current densities of 0.11 mA cm^{-2} and 0.32 mA cm^{-2} were observed with the brush and felt electrode (Figure 3 K, L). The oxidation of the mediator ($K_4Fe(CN)_6$) was similar with all electrodes. Citrate was metabolised linearly for all electrodes (Figure 3 A-C) which usually indicates a limitation.

This limitation was not caused by the availability of $K_3Fe(CN)_6$ since the $K_3Fe(CN)_6$ concentration did not decrease below 2 mM with all electrodes during the processes. Furthermore this limitation was not caused by the electrode surface area since the electrodes with large surface areas showed no benefit. The observed limitation can be explained by the biofilm formation on the surface area of the brush and felt electrode and their pore diffusion resistance. Both factors reduce mass transfer of mediator, substrate and products. It can be assumed that in porous electrodes the outer electrode surface area exposed to the medium mainly contributes to the electron transfer reaction in mediated bio-electrochemical systems while the contribution of the inner specific surface area of porous electrodes is only little due

to mass transfer limitations. In literature, the formation of biofilms on electrodes is often observed and desired [39]. If biofilms form the area at which the bio-electrochemical reaction can take place increases. Increasing the catalytic surface area – which is the surface of the anode that is covered with biofilm - represents one approach to reduce mass transfer limitations. However diffusion of substrate, products and mediator can rapidly become limiting with increasing biofilm thickness [40]. Therefore biofilm thickness has to be controlled. In this study, the anodic respiration of *P. putida* was evaluated with the graphite rod working electrode to simplify the investigation. Effects of biofilm formation such as a changing electrode surface area and diffusion resistances through the biofilm could be neglected because no biofilm formation was visually observed. Furthermore, the effects of high porous electrodes such as pore diffusion resistances did not have to be considered because the graphite rod is non-porous. Also the graphite rod electrode has a very well defined geometry and can be positioned precisely which allows an accurate analysis of the process. Also, the achieved current densities were high and external electron transfer was not limited at any time. Therefore the possibility of a mass transfer limitation was investigated in the following using this electrode.

3.3 Effects of enhanced mass transfer on anodic respiration

The effects of mass transfer on the anodic respiration of *P. putida* KT2440 Δ*pobA*/pSEVA-*ubiC* were studied with two batch experiments using graphite rod electrodes with varied stirrer speeds. The stirrer speed was increased stepwise from 400 rpm beginning at a process time of 120 h to 700 rpm after 150 h (Figure 4 A). In the reference experiment, a constant stirrer speed of 400 rpm was applied. As consequence of increased mass transfer due to increased stirrer speeds, the biomass concentration doubled between 120 h and 150 h and the *p*HBA concentration increased (Figure 4 C). Between 150 h and 250 h biomass growth could be observed (Figure 4 E). During this time $K_3Fe(CN)_6$ was manually added to prevent

complete reduction (Figure 4 D, F, G) leading to a maximal mediator concentration of 43 mM by the end of the batch process (Figure 4 G). Citrate was completely metabolised within 120 h after the first stirrer speed increase (Figure 4 A, B) resulting in a biomass yield of 0.14 $molC_X$ $molC^{-1}_{citrate}$. 100 h before substrate depletion the maximal current density of 8.57 mA cm^{-2} was measured (Figure 4 D). In comparison to the reference batch experiment performed at 400 rpm, biomass yield and current densities were increased by factors of 14 from 0.01 $molC_X$ $molC^{-1}_{citrate}$ to 0.14 $molC_X$ $molC^{-1}_{citrate}$ and of 9.5 from 0.91 mA cm^{-2} to 8.57 mA cm^{-2}, respectively. The specific citrate uptake rate was increased from 0.42 mmol $(g_X\ h)^{-1}$ to 0.66 mmol $(g_X\ h)^{-1}$. Thus increasing mass transfer by increasing the stirrer speed (volumetric power input) enabled faster anodic electro-fermentation.

3.4 Effects of the redox potential in the medium on anodic respiration

By the end of the reference process a *p*HBA yield of 0.14 $mmolC_{pHBA}$ $molC^{-1}_{citrate}$ were reached whereas in the batch process performed at increased stirrer speed no *p*HBA could be detected (Figure 4 C). *p*HBA concentrations started to decrease at 170 h. At this time the ratio of $K_3Fe(CN)_6$ to $K_4Fe(CN)_6$ was 0.08 mM mM^{-1} ($ln(c_{K3Fe(CN)6}/c_{K4Fe(CN)6})$ = -2.5) (Figure 4 F). A ratio of 2.5 mM mM^{-1} ($ln(c_{K3Fe(CN)6}/c_{K4Fe(CN)6})$ = 0.95) was measured in the reference process. The ratio in the reference process decreased slowly to 0.44 mM mM^{-1} ($ln(c_{K3Fe(CN)6}/c_{K4Fe(CN)6})$ = -0.82). The ratios between both experiments therefore differed by a factor of at least 5.5. The simultaneous decline of the ratio of oxidised to reduced mediator species (Figure 3 F) and the *p*HBA concentration (Figure 3 C) hints at a possible connection. An explanation can be given by differentiating between the potential of the working electrode and the redox potential in the medium. The potential of the working electrode affects cells that can transfer their electrons by a direct external electron transfer mechanism and mediator species in the vicinity of the electrode, thereby defining which redox reactions are possible at the electrode. Throughout the process the potential of the anode is constant (as set by the

potentiostat) ensuring the regeneration of the oxidised mediator. In the liquid medium (i.e. at larger distance from the electrode) two redox half reactions are taking place determining the redox potential in the medium: I: $S \rightarrow P + X + z\ e^-$ and II: $M_{red} \rightarrow M_{ox} + z\ e^-$. The subtraction of reaction I and II gives the reaction for substrate to product conversion catalyzed by the microorganism: $S + M_{ox} \rightarrow P + X + M_{red}$. (*S*: substrate; *P*: products; *X*: biomass; M_{ox}: oxidized mediator; M_{red}: reduced Mediator). Each half reaction possesses its own potential E_I and E_{II}. The driving force of this redox system (E_{Medium}) can be calculated: $E_{Medium} = E_I - E_{II}$. If $E_I = E_{II}$ an equilibrium is obtained and the potential in the medium is in the thermodynamic equilibrium (E^0_{Medium}). E^0_{Medium} can be calculated by the Nernst equation as follows:

$$E^0_{Medium} = E^0_I - E^0_{II} = \frac{R \cdot T}{z \cdot F} \ln\left(\frac{K_{II}}{K_I}\right) = \frac{R \cdot T}{z \cdot F} \ln\left(\frac{[M_{ox}] \cdot [e^-]^z \cdot [S]}{[M_{red}] \cdot [P] \cdot [X] \cdot [e^-]^z}\right) = \frac{R \cdot T}{z \cdot F} \ln\left(\frac{[M_{ox}] \cdot [S]}{[M_{red}] \cdot [P] \cdot [X]}\right).$$

(E^0_i: redox potential of reaction in the equilibrium; [*S*]: substrate concentration; [*P*]: products concentration; [*X*]: biomass concentration). Although this equation is only valid in the thermodynamic equilibrium which cannot be reached in living cells (because living is characterized by maintaining a steady state outside the thermodynamic equilibrium and death occurs if the thermodynamic equilibrium is reached [41,42], this equation shows that the redox potential in the medium is a function of the ratio of oxidized to reduced mediator concentration as well as microbial metabolic activity. The ratio of oxidized to reduced mediator can be measured and controlled in a bio-electrochemical system and variations of the redox potential in the medium shifted the product spectrum of *Clostridium acetobutylicum* significantly [43]. In agreement with this, it can be assumed that the decline of the *p*HBA concentration observed in this study occurred simultaneously with the decline of the redox potential in the medium.

For detailed analysis of this issue, an additional redox probe was installed in the anodic chamber of the stirred-tank bioreactor. The redox probe allows to consider the combined effects of mediator, microorganism, pH and any by-products on the redox potential in the medium. The redox potential in the medium is referred to Ag/AgCl. Before inoculation an initial redox potential (E_{Medium}) of 375 mV was measured in the defined medium with 3 mM $K_3Fe(CN)_6$ (Figure 5 A). Four different process phases were observed in the electro-fermentative batch process during citrate conversion with *P. putida* KT2440 Δ*pobA*/pSEVA-*ubiC*. During phase I starting with the inoculation, the cells were in a metabolic state which allowed a fast consumption of citrate (Figure 5 B). The current density increased rapidly (Figure 5 D) and the redox potential in the medium dropped by 74 mV (Figure 5 A). After a process time of 6 h *p*HBA formation was observed (Figure 5 C), whereas by-product formation (malate, fumarate and an unidentified compound) was initiated directly with citrate consumption (Figure 5 F, I, J). At the beginning of phase II (14 h) the formation of the unidentified compound suddenly decreased sharply (Figure 5 J). Furthermore citrate consumption as well was *p*HBA and fumarate formation slowed down whereas a steady formation of malate could be observed and the decreasing biomass concentration approached a constant value (Figure 5 B, C, E, F, I). At this point the cells entered a second metabolic state. The citrate uptake declined after 40 h whereas the formation of fumarate showed a steady decrease until a constant concentration of 1.75 mg L^{-1} was measured at the beginning of phase III (Figure 5 B, I). During phase III the cells shifted to a third metabolic state. Phase III started with increasing citrate uptake (Figure 5 B). As a consequence the current density increased (Figure 5 D). During this time the redox potential in the medium decreased again by 30 mV to 271 mV (Figure 5 A) and by the end of phase III citrate consumption slowed down again (Figure 5 B) leaving the cells in a fourth metabolic state.

3.5 Identification of optimal process conditions for anodic *p*HBA formation

The results indicate that the redox potential in the medium is directly influenced by the metabolic activity of *P. putida*. By controlling the redox potential in the medium at a constant setpoint it might be possible to extend phases of higher metabolic activity and thus optimize *p*HBA-production. In order to identify both a redox potential in the medium and a stirrer speed for which improved *p*HBA formation can be observed, the stirrer speed was changed in the following 480 h of this anodic batch process while the redox potential in the medium was measured. The highest metabolic activity was observed at a stirrer speed of 700 rpm and redox potentials in the medium between 264 mV and 178 mV (vs. Ag/AgCl) (Figure 6 A). Under these conditions increasing biomass, malate and *p*HBA formation as well as citrate uptake was observed (Figure 6 C, E, F). Fumarate was metabolised (Figure 6 I), a markedly increasing current density was observed and $K_3Fe(CN)_6$ concentration decreased (Figure 6 D, G, H).

3.6 Electro-fermentative *p*HBA production at optimal process conditions

To improve the electro-fermentative production of *p*HBA, a batch process was performed where the stirrer speed was set to 700 rpm and the redox potential in the medium was controlled at 225 mV (Figure 7 A) by feeding of $K_3Fe(CN)_6$. $K_3Fe(CN)_6$ concentration was thus increased from 0 mM to 100 mM at the end of the batch process (Figure 7 H). During the initial 420 h citrate was metabolised with a constant rate of 0.21 mmol $(g_X\ h)^{-1}$. Most of the citrate consumed was directly converted to malate (Figure 7 B, F). The maximal malate yield (0.84 $molC_{malate}\ molC^{-1}_{citrate}$) was obtained at a process time of 300 h. In the following malate formation decreased and the maximal malate concentration (3.12 g L^{-1}) was measured at a process time of 420 h resulting in a yield of 0.75 $molC_{malate}\ molC^{-1}_{citrate}$. The malate concentration started to decrease at a process time of 420 h. The co-metabolisation of malate and citrate resulted in significantly increasing *p*HBA and biomass concentrations (Figure 7 C,

E). A final *p*HBA concentration of 36.1 mg L^{-1} (9.91 $mmolC_{pHBA}$ $molC^{-1}_{citrate}$) was achieved and the biomass concentration increased by 0.32 g L^{-1} resulting in a final biomass yield of 0.07 $molC_X$ $molC^{-1}_{citrate}$. The maximal specific *p*HBA formation rate was 0.003 mmol $(g_X\ h)^{-1}$, the maximal growth rate 0.01 h^{-1} and the maximal specific citrate uptake rate 0.30 mmol $(g_X\ h)^{-1}$.

Thus the *p*HBA yields exceeded *p*HBA yields obtained at 400 rpm without medium redox potential control (0.14 $mmolC_{pHBA}$ $molC^{-1}_{citrate}$) by a factor of 72. By controlling the medium redox potential, the metabolisation of *p*HBA which was previously (Figure 4 C) observed at high $K_4Fe(CN)_6$ concentrations and 700 rpm could be avoided (Figure 7 C). Furthermore *p*HBA yields could be increased by 69 % in comparison to the aerobic batch process. In comparison to the aerobic process specific *p*HBA formation, growth and citrate uptake rates were reduced by a factor of 10. A limitation of the diffusion of $K_3Fe(CN)_6$ over the outer cell membrane is unlikely since $K_3Fe(CN)_6$ has a molar weight of 212 g mol^{-1} and is therefore small enough to diffuse through porins such as OmpF which have an exclusion size of 600 kDa [44]. Furthermore mass transfer limitations were significantly reduced. It could therefore be assumed that the metabolism is ATP limited during the electro-fermentation as suggested by theoretical considerations [45]. This would explain lower biomass concentrations as well as slower specific rates in the bio-electrochemical process.

Just before substrate depletion a maximal current density of 12.5 mA cm^{-2} was measured (Figure 7 D) which is the highest ever measured for a bio-electrochemical system with non-porous working electrodes. With non-porous materials such as glassy carbon and graphite rods or plates current densities reported were about 1 mA cm^{-2} at the maximum [46–48]. The maximal current density of 12.5 mA cm^{-2} observed in this study exceeds those by more than one decade. Current densities of 12.87 mA cm^{-2} (ice-templated titanium-based ceramics, [49]) and 39 mA cm^{-2} (layered corrugated carbon, [46]) have been reported for highly porous

anodes. Highly porous electrodes have a significant larger surface area compared to the smooth graphite rod used in this study. While the large surface area of highly porous anodes would theoretically allow better mass transfer due to the increased electrode-electrolyte interface area, in practice the mass transfer enhancement is limited by biofilm formation on the porous surface which impairs mass transfer. The high current density observed in our study can accordingly be attributed to both the absence of a biofilm on the rod electrode and the reduction of mass transfer limitations by the intensive mixing which is possible in the modified stirred-tank bioreactor.

Control of the redox potential in the medium allowed stable metabolisation of citrate by *P. putida* KT2440 Δ*pobA*/pSEVA-*ubiC*. Malate could be identified as the major by-product with a maximum malate yield of 1.26 mole malate per mole citrate at a process time of 300 h.

4 Conclusion

A fully controlled stirred-tank bioreactor can be reversibly transformed into a bio-electrochemical system. Increasing mass transfer by increasing the stirrer speed (volumetric power input) can enable faster anodic electro-fermentations. Control of the redox potential in the medium can be used to improve stable anodic respiration. Combining both approaches enhanced anodic respiration, product formation and current densities significantly.

Proper control of the redox potential in the medium by feeding of mediator and increased power input to minimize mass transfer limitations, combined with optimised working electrode materials and engineered microorganisms will lead to improvements of electro-fermentations. More than any previous reactor, the stirred tank-based bio-electrochemical system described here will enable reliable reaction engineering analysis and support comparability between results.

5 Acknowledgments

The authors would like to express their gratitude to Markus Brammen (Bioseperation Engineering Group, Technical University of Munich) for support with BET measurements. Assistance from Tuan Nygen Khac, Felix Block, Johanna Göbel, Luisa Metzler, Christian Preischel and Lukas Franzgrote is gratefully acknowledged.

Funding: This work was supported by the International Graduate School of Science and Engineering (IGSSE) at the Technical University of Munich (funded by the German Research Foundation DFG).

The authors declare that there is no conflict of interest regarding the publication of this paper.

6 References

[1] R.A. Weusthuis, I. Lamot, J. van der Oost, J.P.M. Sanders, Microbial production of bulk chemicals: development of anaerobic processes, Trends in Biotechnology 29 (2011) 153–158.

[2] R. Ulber, D. Sell, White biotechnology, Springer, Berlin, New York, 2007.

[3] A. Singh, K. Cher Soh, V. Hatzimanikatis, R.T. Gill, Manipulating redox and ATP balancing for improved production of succinate in *E. coli*, Metabolic Engineering 13 (2011) 76–81.

[4] K.-K. Cheng, G.-Y. Wang, J. Zeng, J.-A. Zhang, Improved succinate production by metabolic engineering, BioMed research international 2013 (2013) 538790.

[5] R. Liu, L. Liang, K. Chen, J. Ma, M. Jiang, P. Wei, P. Ouyang, Fermentation of xylose to succinate by enhancement of ATP supply in metabolically engineered Escherichia coli, Applied Microbiology and Biotechnology 94 (2012) 959–968.

[6] S.Y. Lee, S.H. Hong, S.Y. Moon, In silico metabolic pathway analysis and design: succinic acid production by metabolically engineered Escherichia coli as an example, Genome informatics. International Conference on Genome Informatics 13 (2002) 214–223.

[7] M.A. Rosenbaum, A.E. Franks, Microbial catalysis in bioelectrochemical technologies: status quo, challenges and perspectives, Appl Microbiol Biotechnol 98 (2014) 509–518.

[8] F. Kracke, J.O. Krömer, Identifying target processes for microbial electrosynthesis by elementary mode analysis, BMC bioinformatics 15 (2014) 410.

[9] A.V. Pandit, R. Mahadevan, In silico characterization of microbial electrosynthesis for metabolic engineering of biochemicals, Microbial cell factories 10 (2011) 76.

[10] H.S. Shin, J.G. Zeikus, M.K. Jain, Electrically enhanced ethanol fermentation by *Clostridium thermocellum* and *Saccharomyces cerevisiae*, Applied Microbiology and Biotechnology 58 (2002) 476–481.

[11] T.S. Kim, B.H. Kim, Electron flow shift in *Clostridium acetobutylicum* fermentation by electrochemically introduced reducing equivalent, Biotechnol Lett 10 (1988) 123–128.

[12] D.H. Park, J.G. Zeikus, Utilization of electrically reduced neutral red by *Actinobacillus succinogenes*: Physiological function of neutral red in membrane-driven fumarate reduction and energy conservation, Journal of bacteriology 181 (1999) 2403–2410.

[13] K. Sturm-Richter, F. Golitsch, G. Sturm, E. Kipf, A. Dittrich, S. Beblawy, S. Kerzenmacher, J. Gescher, Unbalanced fermentation of glycerol in *Escherichia coli* via heterologous production of an electron transport chain and electrode interaction in microbial electrochemical cells, Bioresource Technology 186 (2015) 89–96.

[14] J.O. Krömer, D. Nunez-Bernal, N.J.H. Averesch, J. Hampe, J. Varela, C. Varela, Production of aromatics in Saccharomyces cerevisiae—A feasibility study, From Gene to ProductFrom Gene to Product 163 (2013) 184–193.

[15] J.L. Barker, J.W. Frost, Microbial synthesis of *p* - hydroxybenzoic acid from glucose, Biotechnol. Bioeng. 76 (2001) 376 – 390.

[16] J.O. Krömer, D. Nunez-Bernal, N.J. Averesch, J. Hampe, J. Varela, C. Varela, Production of aromatics in Saccharomyces cerevisiae—A feasibility study, Journal of Biotechnology 163 (2013) 184–193.

[17] T.C. Williams, N. Averesch, G. Winter, M.R. Plan, C.E. Vickers, L.K. Nielsen, J.O. Krömer, Quorum-sensing linked RNA interference for dynamic metabolic pathway control in Saccharomyces cerevisiae, Metabolic Engineering 29 (2015) 124–134.

[18] S. Verhoef, H. Ballerstedt, R.J.M. Volkers, J.H. Winde, H.J. Ruijssenaars, Comparative transcriptomics and proteomics of *p*-hydroxybenzoate producing *Pseudomonas putida* S12:

novel responses and implications for strain improvement, Appl Microbiol Biotechnol 87 (2010) 679–690.

[19] J.-P. Meijnen, S. Verhoef, A.A. Briedjlal, J.H. Winde, H.J. Ruijssenaars, Improved *p*-hydroxybenzoate production by engineered *Pseudomonas putida* S12 by using a mixed-substrate feeding strategy, Appl Microbiol Biotechnol 90 (2011) 885–893.

[20] S. Collado, I. Rosas, C. González, M. Diaz, Biodegradation of *p*-hydroxybenzoic acid by *Pseudomonas putida*, Desalination and Water Treatment (2015) 1–11.

[21] M.-I. Ramos-Gonzalez, A. Ben-Bassat, M.-J. Campos, J.L. Ramos, Genetic engineering of a highly solvent-tolerant *Pseudomonas putida* strain for biotransformation of toluene to *p*-hydroxybenzoate, Applied and Environmental Microbiology 69 (2003) 5120–5127.

[22] K. Rabaey, R.A. Rozendal, Microbial electrosynthesis - revisiting the electrical route for microbial production, Nat Rev Micro 8 (2010) 706–716.

[23] S.A. Patil, C. Hägerhäll, Lo Gorton, Electron transfer mechanisms between microorganisms and electrodes in bioelectrochemical systems, Bioanal Rev 4 (2012) 159–192.

[24] T. Ikeda, T. Kurosaki, K. Takayama, K. Kano, K. Miki, Measurements of Oxidoreductase-like Activity of Intact Bacterial Cells by an Amperometric Method Using a Membrane-Coated Electrode, Anal. Chem. 68 (1996) 192–198.

[25] B. Lai, S. Yu, P.V. Bernhardt, K. Rabaey, B. Virdis, J.O. Krömer, Anoxic metabolism and biochemical production in *Pseudomonas putida* F1 driven by a bioelectrochemical system, Biotechnology for Biofuels 9 (2016) 39.

[26] T. Krieg, A. Sydow, U. Schröder, J. Schrader, D. Holtmann, Reactor concepts for bioelectrochemical syntheses and energy conversion, Trends in Biotechnology 32 (2014) 645–655.

[27] E. Martinez-Garcia, V. de Lorenzo, Engineering multiple genomic deletions in Gram-negative bacteria: analysis of the multi-resistant antibiotic profile of Pseudomonas putida KT2440, Environmental Microbiology 13 (2011) 2702–2716.

[28] R. Silva-Rocha, E. Martinez-Garcia, B. Calles, M. Chavarria, A. Arce-Rodriguez, de Las Heras, Aitor, A.D. Paez-Espino, G. Durante-Rodriguez, J. Kim, P.I. Nikel, R. Platero, V. de Lorenzo, The Standard European Vector Architecture (SEVA): a coherent platform for the analysis and deployment of complex prokaryotic phenotypes, Nucleic acids research 41 (2013) D666-75.

[29] K.-H. Choi, H.P. Schweizer, mini-Tn7 insertion in bacteria with single attTn7 sites: example Pseudomonas aeruginosa, Nature protocols 1 (2006) 153–161.

[30] J.R. Kim, S. Cheng, S.-E. Oh, B.E. Logan, Power generation using different cation, anion, and ultrafiltration membranes in microbial fuel cells, Environ. Sci. Technol. 41 (2007) 1004–1009.

[31] J.X. Leong, Daud, Wan Ramli Wan, M. Ghasemi, K.B. Liew, M. Ismail, Ion exchange membranes as separators in microbial fuel cells for bioenergy conversion: A comprehensive review, Renewable and Sustainable Energy Reviews 28 (2013) 575–587.

[32] M. Rahimnejad, A. Adhami, S. Darvari, A. Zirepour, S.-E. Oh, Microbial fuel cell as new technology for bioelectricity generation: A review, Alexandria Engineering Journal 54 (2015) 745–756.

[33] C.A. Appleby, R.K. Morton, Lactic dehydrogenase and cytochrome b_2 of baker's yeast. Purification and crystallization, Biochemical Journal 71 (1959) 492–499.

[34] G.A.F. Seber, C.J. Wild (Eds.), Nonlinear rgression, John Wiley & Sons, Inc, Hoboken, NJ, USA, 1989.

[35] J. van Duuren, J. Puchałka, A.E. Mars, R. Bücker, G. Eggink, C. Wittmann, dos Santos, Vítor AP, Reconciling in vivo and in silico key biological parameters of *Pseudomonas putida* KT2440 during growth on glucose under carbon-limited condition, BMC Biotechnol 13 (2013) 93.

[36] S. Schmitz, S. Nies, N. Wierckx, L.M. Blank, M.A. Rosenbaum, Engineering mediator-based electroactivity in the obligate aerobic bacterium *Pseudomonas putida* KT2440, Frontiers in Microbiology 6 (2015).
[37] P. Duboc, N. Schill, L. Menoud, W. van Gulik, U. von Stockar, Measurements of sulfur, phosphorus and other ions in microbial biomass: Influence on correct determination of elemental composition and degree of reduction, Journal of Biotechnology 43 (1995) 145–158.
[38] M. Sharma, S. Bajracharya, S. Gildemyn, S.A. Patil, Y. Alvarez-Gallego, D. Pant, K. Rabaey, X. Dominguez-Benetton, A critical revisit of the key parameters used to describe microbial electrochemical systems, Electrochimica Acta (2014).
[39] B. Erable, N.M. Duţeanu, M.M. Ghangrekar, C. Dumas, K. Scott, Application of electro-active biofilms, Biofouling 26 (2010) 57–71.
[40] P.S. Stewart, Diffusion in biofilms, Journal of bacteriology 185 (2003) 1485–1491.
[41] L.M. Balakireva, V.M. Kantere, I.L. Rabotnova, The redox potential in microbiological media, Biotechnology and bioengineering symposium 0 (1974) 769–780.
[42] L. Kjaergaard, The redox potential: Its use and control in biotechnology, Advances in Biochemical Engineering 7 (1977) 131–150.
[43] S. Peguin, P. Soucaille, Modulation of metabolism of *Clostridium acetobutylicum* grown in chemostat culture in a three-electrode potentiostatic system with methyl viologen as electron carrier, Biotechnology and bioengineering 51 (1996) 342–348.
[44] P. Dersch, K. Munk, Mikrobiologie: 43 Tabellen, Thieme, Stuttgart, 2008.
[45] F. Kracke, I. Vassilev, J.O. Krömer, Microbial electron transport and energy conservation - the foundation for optimizing bioelectrochemical systems, Front. Microbiol. 6 (2015) 101.
[46] S. Chen, G. He, Q. Liu, F. Harnisch, Y. Zhou, Y. Chen, M. Hanif, S. Wang, X. Peng, H. Hou, U. Schröder, Layered corrugated electrode macrostructures boost microbial bioelectrocatalysis, Energy Environ. Sci. 5 (2012) 9769.
[47] S.F. Ketep, A. Bergel, A. Calmet, B. Erable, Stainless steel foam increases the current produced by microbial bioanodes in bioelectrochemical systems, Energy Environ. Sci. 7 (2014) 1633.
[48] S. Chen, H. Hou, F. Harnisch, S.A. Patil, A.A. Carmona-Martinez, S. Agarwal, Y. Zhang, S. Sinha-Ray, A.L. Yarin, A. Greiner, U. Schröder, Electrospun and solution blown three-dimensional carbon fiber nonwovens for application as electrodes in microbial fuel cells, Energy Environ. Sci. 4 (2011) 1417.
[49] D. Massazza, R. Parra, J.P. Busalmen, H.E. Romeo, New ceramic electrodes allow reaching the target current density in bioelectrochemical systems, Energy Environ. Sci. 8 (2015) 2707–2712.

List of Figures

Figure 1 Modified stirred-tank bioreactor used as bio-electrochemical reactor. A: Schematic drawing of the 1.8 L reactor vessel. WE: working electrode; RE: reference electrode; CE: counter electrode. Materials used for the modifications are indicated by colour coding. Red: glass, Green: PEEK, Blue: PVC and silicone. B: Photo of the assembled reactor. C: Photo of the lid with modifications. D: Schematic drawing of the custom-made cathode chamber. E: Photo of the cathode chamber. F: Schematic drawing of the reference electrode and bridge tube. G: Photo of reference electrode and bridge tube.

Figure 2 Aerobic batch conversion of citrate with *P. putida* KT2440 Δ*pobA*/pSEVA-*ubiC* in an aerated stirred-tank bioreactor at 30°C, stirrer speed = 400 - 700 rpm, pH 7, working volume = 1 L (A, B, C: symbols - measured concentrations, lines - interpolated concentrations; D, E, F: estimated rates based on interpolated concentrations; G, H, I: measured data; J, K, L: estimated rates based on interpolated biomass data; M, N: carbon and electron balances based on measured concentrations).

Figure 3 Electro-fermentative batch conversion of citrate with *P. putida* KT2440 Δ*pobA*/pSEVA-*ubiC*: Effects of different electrodes on anodic respiration. Electrodes: Graphite rod (○), graphite brush (□), graphite felt (Δ).

Figure 4 Electro-fermentative batch conversion of citrate with *P. putida* KT2440 Δ*pobA*/pSEVA-*ubiC*: Effects of increased stirrer speeds and mediator

concentrations on anodic respiration. Constant stirrer speed: Dashed line and □; Increased stirrer speed: thick black line and ■. Arrows in panel D indicate manual replenishment with $K_3Fe(CN)_6$.

Figure 5 Electro-fermentative batch conversion of citrate with *P. putida* KT2440 Δ*pobA*/pSEVA-*ubiC*: Effects of the redox potential in the medium on anodic respiration. 400 rpm, 3 mM $K_3Fe(CN)_6$, graphite rod working electrode, E_{WE} = 0.500 V.

Figure 6 Electro-fermentative batch conversion of citrate with *P. putida* KT2440 Δ*pobA*/pSEVA-*ubiC*: Measurement of redox potential in the medium at varying stirrer speeds during electro-fermentative production of *p*HBA. A: stirrer speed (dashed line) and redox potential in the medium E_{Medium} (black line). Grey background: Reaction conditions where fast and steady *p*HBA formation was observed.

Figure 7: Electro-fermentative batch conversion of citrate with *P. putida* KT2440 Δ*pobA*/pSEVA-*ubiC*: Electro-fermentation with a stirrer speed of 700 rpm and control of the redox potential in the medium at 225 mV. A: Stirrer speed (dashed line) and redox potential in the medium (black line).

List of Tables

Table 1 Projected, geometric and specific surface areas of the three electrodes used in this study. Projected surface areas of all electrodes were rectangular. Geometric surface areas were approximated by a cylinder (rod and brush electrode) and a cuboid (felt electrode). Specific surface areas were determined by BET measurements. The photos show graphite rod, graphite felt and graphite brush electrode before and after anodic electro-fermentation with *P. putida* KT2440 Δ*pobA*/pSEVA-*ubiC* under anaerobic conditions.

	Graphite rod	Graphite brush	Graphite felt
Projected surface area, cm^2	5.28	22.50	19.87
Geometric surface area, cm^2	18.98	159.00	43.50
Specific surface area, $m^2\ kg^{-1}$	0.750*	299	409
Before anodic application			
After anodic application			

*: Determination based on geometrical surface area and weight.

Figures

Please note that the following figures are embedded into the word document and are – due to limitations in Microsoft Word – of reduced quality.

For high quality versions, please refer to the figures uploaded as separate TIF files.

Figure 1

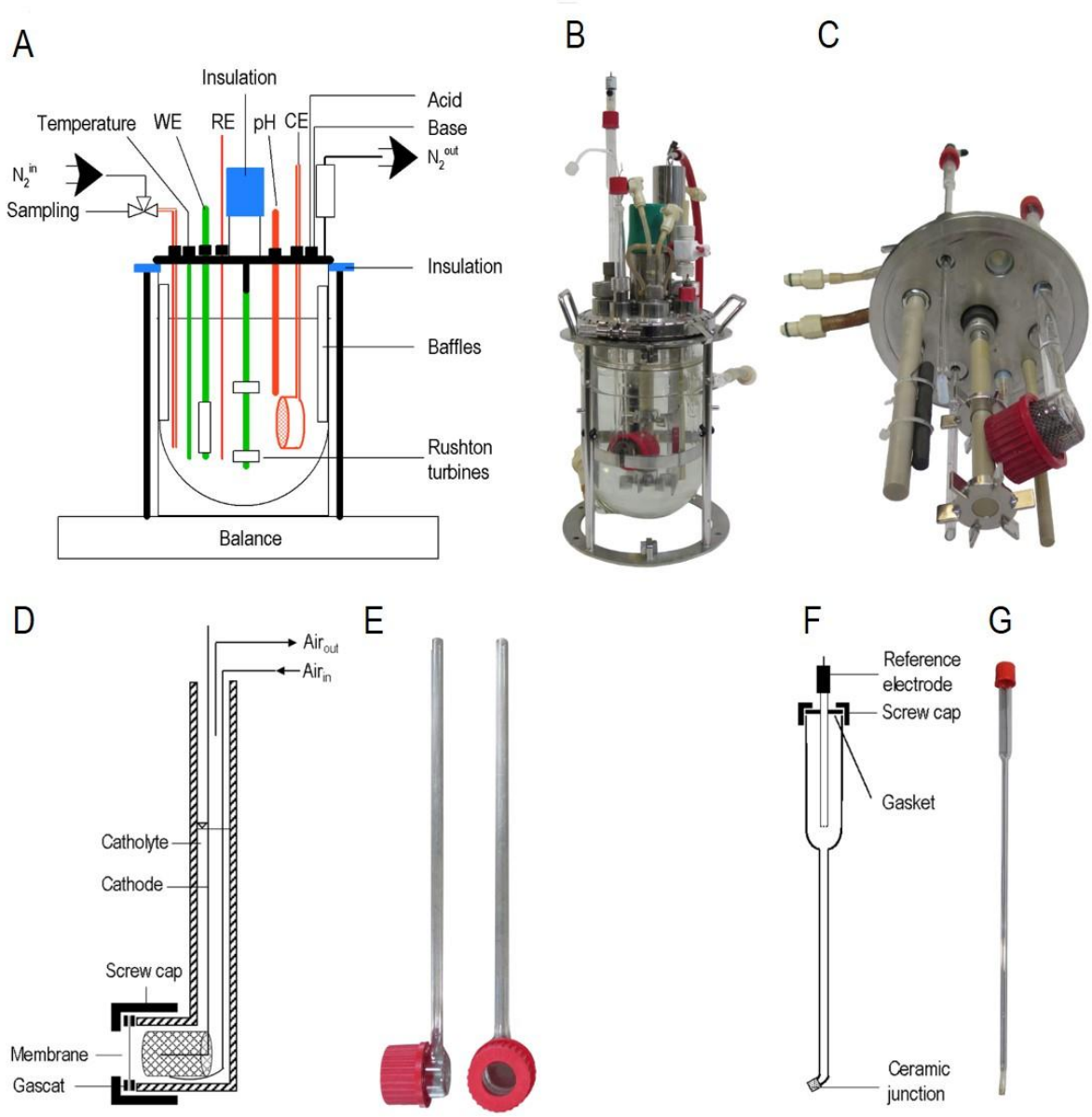

Figure 2

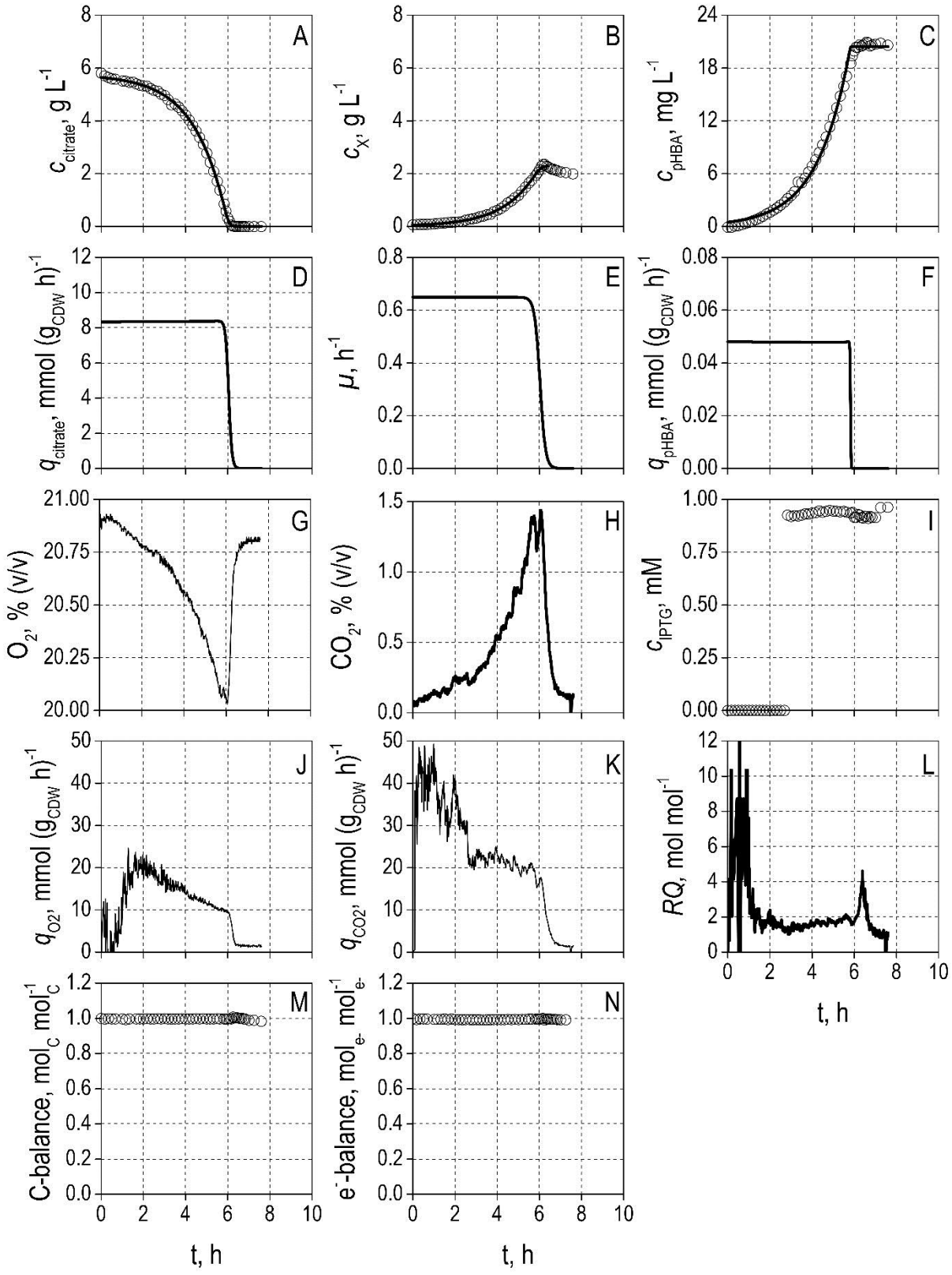

Figure 3

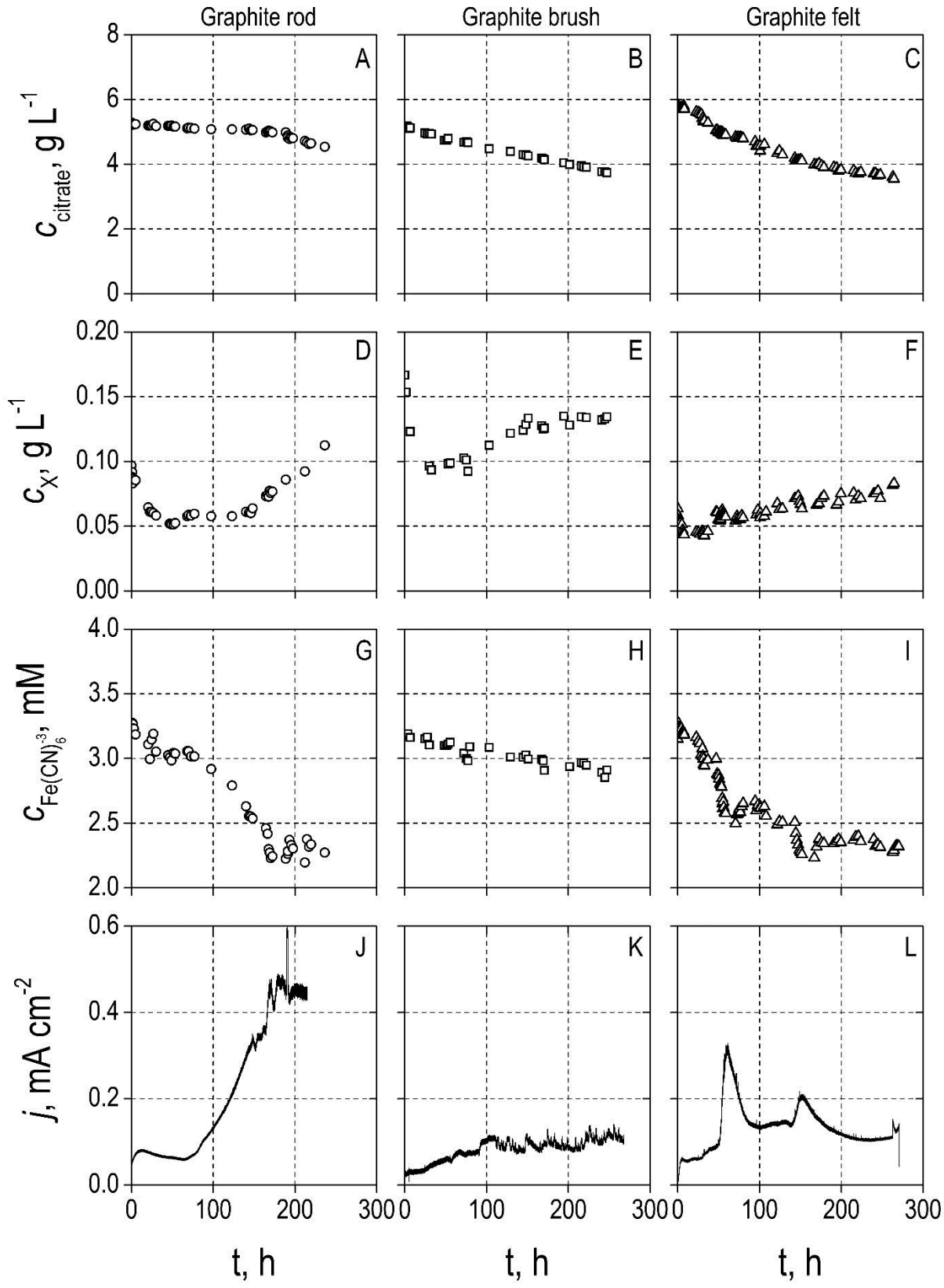

Figure 4

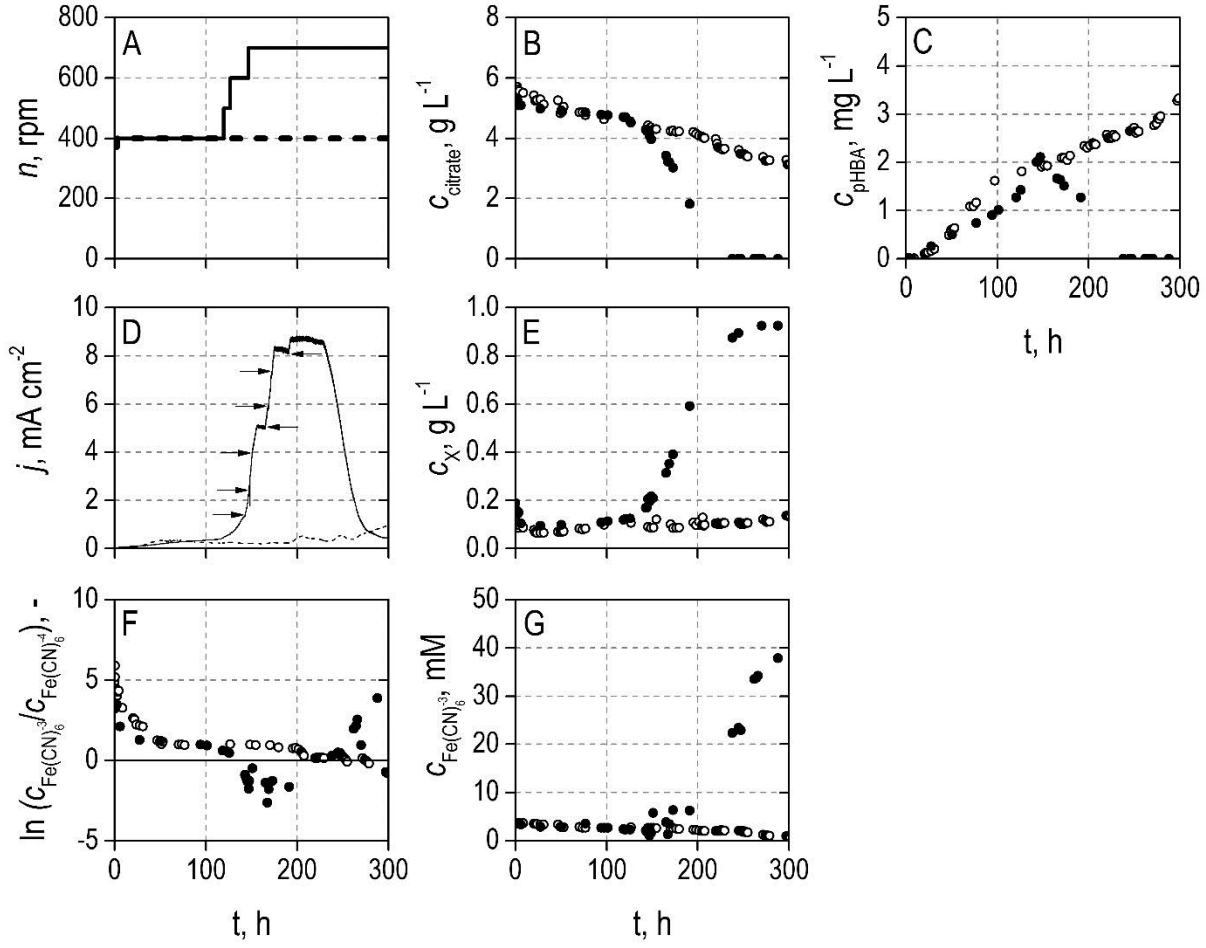

Figure 5

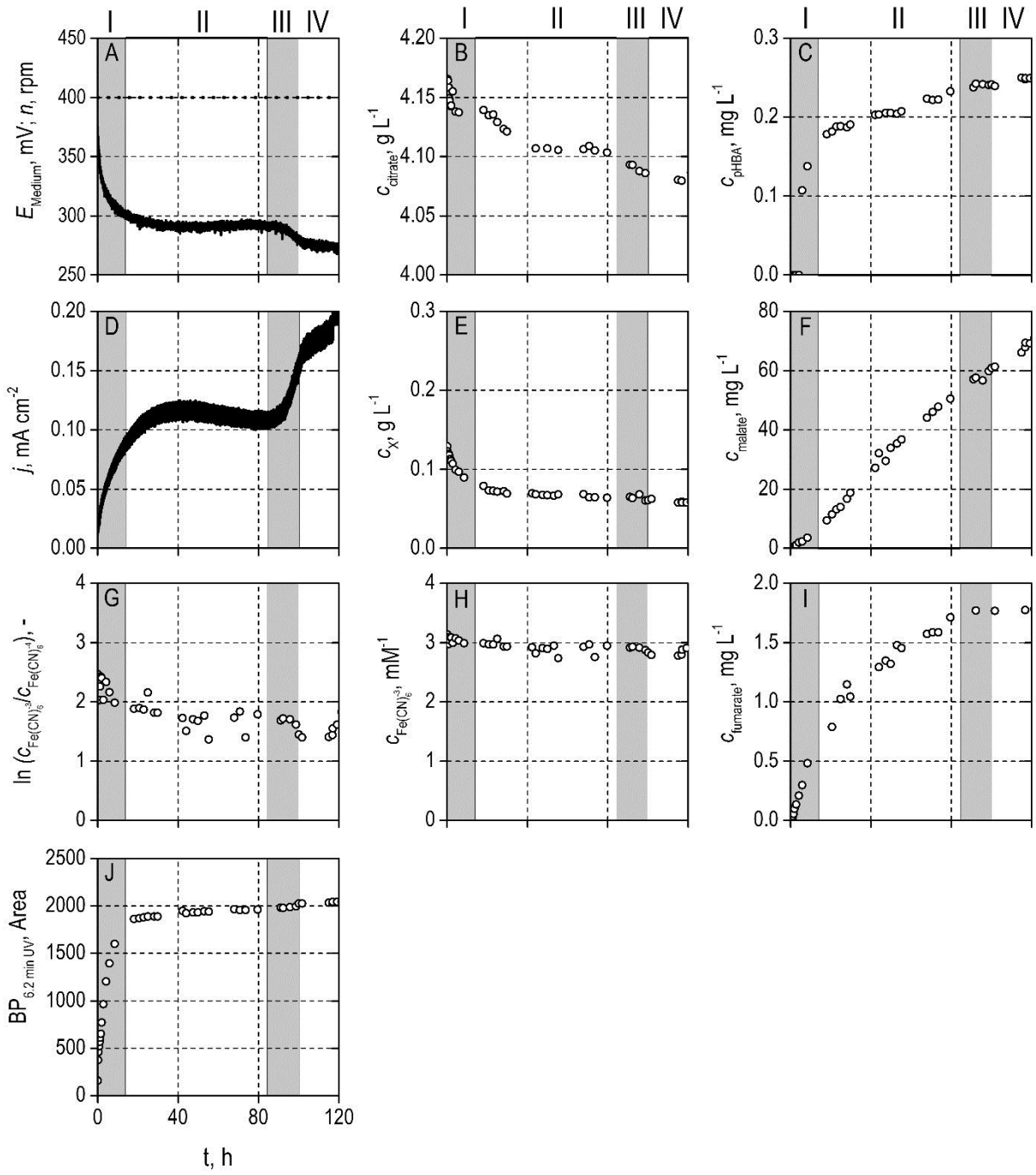

Figure 6

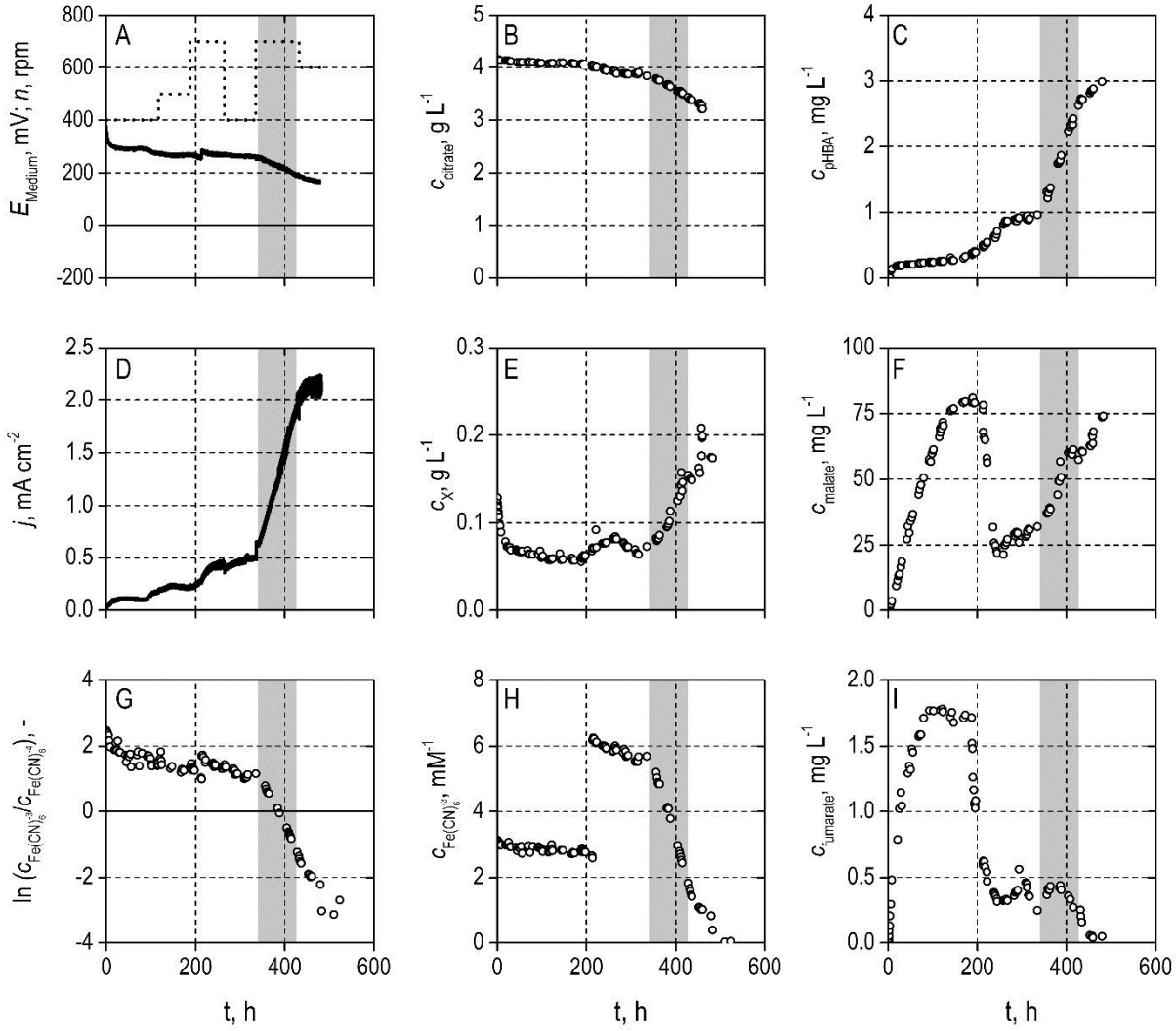

Figure 7